A Closed-Form Expression of Soil Temperature Sensing Depth at L-Band

Shaoning Lv, Yijian Zeng, Zhongbo Su, and Jun Wen

***Abstract*— L-band passive microwave remote sensing is one of the most effective methods to map the global soil moisture distribution, yet, at which soil depth satellites are measuring is still inconclusive. Recently, with the Lv's multilayer soil effective temperature scheme, such depth information can be revealed in the framework of the zeroth-order incoherent model when soil temperature varies linearly with soil optical depth. In this paper, we examine the relationships between soil temperature microwave sensing depth, penetration depth, and soil effective temperature, considering the nonlinear case. The soil temperature sensing depth often also named penetration depth is redefined as the depth where soil temperature equals the soil effective temperature. A method is developed to estimate soil temperature sensing depth from one pair of soil temperature and moisture measurement at an arbitrary depth, the soil surface temperature, and the deep soil temperature which is assumed to be constant in time. The method can be used to estimate the soil effective temperature and soil temperature sensing depth.**

***Index Terms*— Microwave remote sensing, penetration depth, soil effective temperature, soil optical depth, soil temperature sensing depth.**

I. Introduction

SOIL moisture strongly impact the energy and water balance over the land since the heat capacity of wet soil is larger than that of dry soil, and more heat energy can be stored in wet soil. On the other hand, soil moisture can be transferred into water vapor and thus latent heat, which can be transferred to atmosphere by evaporation. This feature makes soil moisture a key variable for the weather forecasting, climate, and agriculture. Many devices exist which measure soil moisture either locally or at the regional scale. L-band microwave remote sensing is recognized as the most promising tool for mapping the regional and global soil moisture distribution [1]–[4] because of the strong relation between soil emissivity and soil moisture at this frequency. Soil heterogeneity, however, makes this relation uncertain. Since the 1970s, the effects of dielectric constant, vegetation, and soil roughness on the observed remote sensing signal have been studied, including radio frequency interference (RFI) and others [5].

The zeroth-order incoherent model is currently the theoretical basis for soil moisture retrieval at L-band, which states that the observed brightness temperature T_B can be written as $T_B = \varepsilon T_{\text{eff}}$ with ε as soil emissivity and T_{eff} as effective soil temperature. However, only a few studies discussed the soil depth to which T_{eff} was referred to. In forward simulations, emissivity is often assumed as the emissivity of the upper layer, while no explicated depth is attributed to that layer. Similarly, satellite soil moisture calibrations/validations usually take soil moisture measurements at a fixed layer. Such fixed depth, however, does not reflect the dynamics of dielectric profile changes due to the change of soil moisture profiles. In reality, surface soil moisture gradients can be very sharp especially after the rainfall. Neglecting such effects will cause uncertainties of soil moisture retrievals at an order of magnitude as large as those caused by roughness and vegetation [6].

Escorihuela *et al.* [7] defined the moisture sensing depth as the soil moisture layer, which has the highest correlation coefficient with T_b. Since the near-surface layers usually contribute most to the emission, its soil moisture is mostly used to compute the emissivity in the radiative transfer models. Zhou *et al.* [8] claimed that the attenuation of radiation by the soil is too weak to make noticeable effects. But, without a clear definition of moisture and temperature sensing depths, it is difficult to quantify the relationship between T_b and soil moisture including its effective depth.

Usually, the microwave penetration depth is assumed to be equal to the soil temperature sensing depth, i.e., the depth at which incoming radiation is reduced to $1/e$ [9]. In this paper, we revisited these concepts of penetration depth and soil temperature sensing depth. Here, we defined the soil temperature sensing depth as the depth at which the soil temperature equals the soil effective temperature. The incoherent model reads

$$T_b = \varepsilon T_{\text{eff}} \tag{1}$$

where T_b is the brightness temperature detected by the radiometer and ε is the soil bulk emissivity which is strongly

Manuscript received October 8, 2018; revised December 3, 2018; accepted December 31, 2018. Date of publication February 21, 2019; date of current version June 24, 2019. The work of S. Lv was supported in part by the National Science Foundation of China under Grant 41530529 and Grant 41575013 and in part by the Chinese Scholarship Council. This work was supported in part by the ESA MOST Dragon IV Program (Monitoring Water and Energy Cycles at Climate Scale in the Third Pole Environment) and in part by the Netherlands Organization for Scientific Research under Project ALW-GO/14-29. *(Corresponding author: Jun Wen.)*

S. Lv is with the Key Laboratory of Land Surface Process and Climate Change in Cold and Arid Region, Northwest Institute of Eco-Environment and Resources, Chinese Academy of Sciences, Lanzhou 730000, China, and also with the Department of Water Resources, Faculty of Geo-Information Science and Earth Observation (ITC), University of Twente, 7500 AE Enschede, The Netherlands (e-mail: s.lv@utwente.nl).

Y. Zeng and Z. Su are with the Department of Water Resources, Faculty of Geo-Information Science and Earth Observation (ITC), University of Twente, 7500 AE Enschede, The Netherlands (e-mail: y.zeng@utwente.nl; z.su@utwente.nl).

J. Wen is with the College of Atmospheric Sciences, Plateau Atmosphere and Environment Key Laboratory of Sichuan Province, Chengdu University of Information Technology, Chengdu 610225, China (e-mail: jwen@cuit.edu.cn).

Color versions of one or more of the figures in this paper are available online at http://ieeexplore.ieee.org.

Digital Object Identifier 10.1109/TGRS.2019.2893687

related to the soil moisture, since its dielectric constant varies from 3 to 80 at L-band (e.g., from dry to wet). The zeroth-order incoherent model is an approximation of the coherent model; thus, the zeroth-order incoherent model and coherent model should lead to the same results if one can find the effective soil temperature and an effective soil moisture for the nonuniform soil moisture and temperature profiles. T_{eff} is a virtual concept and cannot be directly observed but is required to determine the effective emissivity of a soil layer. In the coherent model, reflectivity and absorption are calculated for each layer and thus does not require T_{eff}. It should be noted that T_{eff} can also include canopy temperature in zeroth-order incoherent radiative transfer forward model. The concept of optical depth is widely used in describing vegetation component in forward models.

Based on the zeroth-order incoherent model, only one soil moisture value can be retrieved from the brightness temperature, while T_{eff} needs to consider the effects of soil moisture/temperature gradients. Thus, soil moisture derived from ε cannot be simply attributed to a specific depth. Thus, only T_{eff} is associated with depth and is the parameter in incoherent models for understanding satellite sensing depth.

The calculation of T_{eff} from its integral formula requires the accurate knowledge of both the profiles of temperature and soil moisture [10]. The accuracy also depends on the precision of the dielectric constant model which contains soil moisture and soil temperature to calculate permittivity (the real part) and attenuation (the imaginary part). In practice, these details are neither known in land surface models, which assume uniform soil moisture/temperature values within each layer, nor in used field observations. Choudhury *et al.* [11] developed a simplified form of the integral formula which requires only the surface temperature (0–2 cm) and the deep soil temperature (∼80 cm) besides a constant *C,* which depends on wavelength and was determined from laboratory experiment. Choudhury's scheme proved to work well for C-band (6.9 GHz) but not for L-band (1.4 GHz), the wavelength used by the SMOS and SMAP satellites. Another two T_{eff} schemes were proposed by Wigneron *et al.* [12] and Holmes *et al.* [13] with more specific parameterization of "C". All these schemes are semiempirical based on particular experiment datasets.

Lv *et al.* [14] developed a new T_{eff} scheme (Lv's scheme hereafter), which preserves most of the physics without semiempirical parameters. The scheme gives a physical interpretation of the parameter C and bridges the gap between the two-layer and the integral scheme by accounting for multilayer soil moisture/temperature information [14]. The scheme can also be used to do T_{eff} consistency checks between *in-situ* observation at different depths and SMOS/SMAP observations, by evaluating the contributions from different soil layers. As such, all sorts of specific depth configurations of land surface model or nonuniform field observations can be used in the Lv's scheme [15]. With the scheme, also the relationship between soil moisture and soil temperature profiles can be explored with just a few sampling points along the depth. In [16], we proved that the soil temperature at the penetration depth is equal to T_{eff} when the soil temperature varies linearly with soil optical depth. Here, we will first review this linear assumption and infer the soil optical depth–soil temperature relationship for nonlinear cases. A semiempirical model of soil temperature–soil optical depth scheme is developed and tested against *in-situ* observation at the Maqu network over Tibetan Plateau [17].

II. Methodology and Data

A. Soil Optical Depth and Soil Effective Temperature

Here, we explore the relationship between penetration depth, soil temperature sensing depth, and T_{eff}. This section introduces how the soil geometric depth can be expressed as $1 - e^{-\tau}$ with τ the soil optical depth. In Section II-C, we express the soil temperature profile $T(x)$ as a normalized soil temperature profile $\Delta T_{\text{nor}}(\tau)$ with soil optical depth as coordinate. While Section II-E presents a soil temperature sensing depth estimation method for soil temperature profiles linear in τ, its extension to the nonlinear case is discovered in Section II-D. All variables used in this paper are summarized in Table I.

B. Formulation of T_{eff} in Soil Optical Depth and Transmitting

T_{eff} can be understood as a superposition of the intensities emitted at various depths within the soil. $T_{\text{eff}} = \int_0^\infty T(x)\alpha(x)\exp[-\int_0^x \alpha(x')dx']dx$ with α the volume absorption coefficient of the soil. Assuming a layered soil $\alpha(x)$. Δx is the optical depth $\Delta\tau$ of the particular layer for which holds $\Delta\tau = \Delta x \cdot \alpha(x)$ [16], $\Delta x = (2\pi/\lambda)(\varepsilon''/\sqrt{\varepsilon'})$, and $\exp[-\int_0^x \alpha(x')dx'] = e^{-\tau}$. Thus, T_{eff} can be rewritten as

$$T_{\text{eff}} = \int_0^\infty T[x(\tau)]e^{-\tau}d\tau = \int_0^{+\infty} T(\tau)e^{-\tau}d\tau \tag{2}$$

where τ increases with soil depth. With both soil depth and τ between $[0, +\infty)$, we can define $t = 1 - e^{-\tau} \in [0, 1)$, and further rewrite the equation to

$$T_{\text{eff}} = \int_0^1 T(t)dt. \tag{3}$$

C. Normalization of the Soil Temperature Profile

As we know, the essence of T_{eff} calculation is a series of weights which reflect the soil temperature gradient (for example, the Choudhury's scheme) and further the impact of soil moisture (for example, Wigneron's and Holmes' schemes). Therefore, we can simplify the soil temperature gradient $T(\tau)$ by normalizing them as

$$\Delta T_{\text{nor}}(\tau) = \frac{T(\tau) - T_{\text{surf}}}{T_{\text{deep}} - T_{\text{surf}}} \tag{4}$$

where T_{surf} is the soil temperature at the soil surface. T_{deep} is the soil temperature at the soil bottom where soil temperature could be considered as constant at annual scale. $T(\tau)$ is the physical soil temperature at τ in (3). In summary, a new coordinate of normalized soil temperature versus $1-e^{-\tau}$ (hereafter as $y_{\text{nst}} - x_{1-e^{-\tau}}$ while y_{nst} means "normalized soil temperature"), instead of soil temperature and soil moisture profiles, can be used to help us understand the relationship between T_{eff}

TABLE I
VARIABLES USED IN THIS PAPER

Symbol	Quantity	Unit or Expression
B	The former parameter in Lv's scheme and is replaced by $\Delta\tau$	See Lv et al., 2014
T_{eff}	soil effective temperature	K
T_b	brightness temperature	K
θ	soil moisture	Vol/Vol
$x_{1-e^{-\tau}}$	x-axis with $t=1-e^{-\tau}$	Equation (3)
y_{nst}	y-axis with the normalized soil temperature	Equation (4)
$T(t)$	soil temperature at $y_{nst}-x_{1-e^{-\tau}}$ coordinate where $t=1-e^{-\tau}$	K
$T(\tau)$	soil temperature at soil optical depth τ	K
$T(x)$	soil temperature at physical soil depth x	K
$\Delta T_{nor}(\tau)$	Normalized soil temperature at soil optical depth τ	Equation (4)
$\Delta T_{nor}(t)$	Normalized soil temperature in the $y_{nst}-x_{1-e^{-\tau}}$ coordinate where $t=1-e^{-\tau}$	-
T_{surf}	skin temperature	K
T_{deep}	soil temperature at a deep layer that the soil temperature could be considered as constant	K
a	Soil temperature gradient	K/τ
$\alpha(x)$	attenuation parameter	$\alpha(x)=\frac{4\pi}{\lambda}\varepsilon''(x)\Big/2\left[\varepsilon'(x)\right]^{\frac{1}{2}}$
τ_{deep}	τ deep enough that the soil temperature could be considered as constant	
b	The parameter to adjusting Equation (8) and Equation (7) to cases in Figure 2	Equation (10)
τ_{Teff}	Soil temperature sensing depth	Equation (12)

K =Kelvin; Vol=Volume

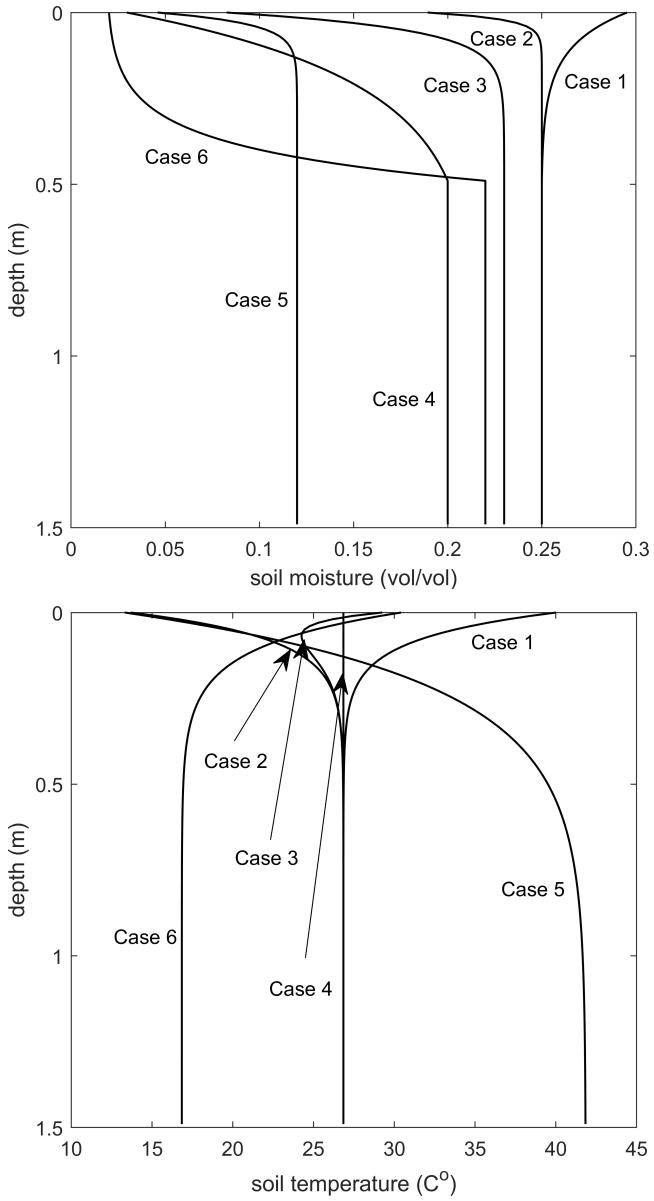

Fig. 1. (Top) Six typical soil moisture and (Bottom) soil temperature profiles. Therefore, it is possible to create 36 dielectric profiles where $\varepsilon = f(\theta, T)$ with different soil temperature/moisture combinations. Details of these profiles can be seen in [9] and [22].

and the soil optical depth. τ strongly relies on soil moisture profile but is also affected by soil temperature profile. The impact of soil temperature on τ is prominent over arid and semiarid areas, where the change of soil moisture content is tightly coupled with soil heat dynamics [18]–[21].

By $\tau = \int_0^x (2\pi/\lambda)(\varepsilon''/\sqrt{\varepsilon'})dx$, τ is related to geometric depth and soil moisture and it is monotonous and accumulative along the soil profile. Fig. 1 shows six typical soil temperature and soil moisture profiles [22]. Soil temperature Profiles 1–4 and 6 represent stages in diurnal heating and cooling of different soil surfaces, respectively. Profile 5 is a profile chosen to investigate the sensitivity of T_{eff} to subsurface temperature anomalies such as occurred in areas of geothermal activities [22]. Among the six typical soil temperature profiles shown in Fig. 1, only Case 3 and Case 4 are not monotonous [22]. For both cases, their vertical average soil temperature variation (not gradient) would be small, which means T_{eff} would be more or less the same as Case 3, i.e., $\overline{(\Delta T/\Delta x)} \approx 0$, and similar to the uniform soil temperature profile in Case 4. Therefore, inferred from (2), $T_{\text{eff}} \approx T(x)$ for soil temperature Case 3 and $T_{\text{eff}} = T(x)$ for Case 4 where x could be at any depth. Cases 3 and 4 will not be discussed in details in the following.

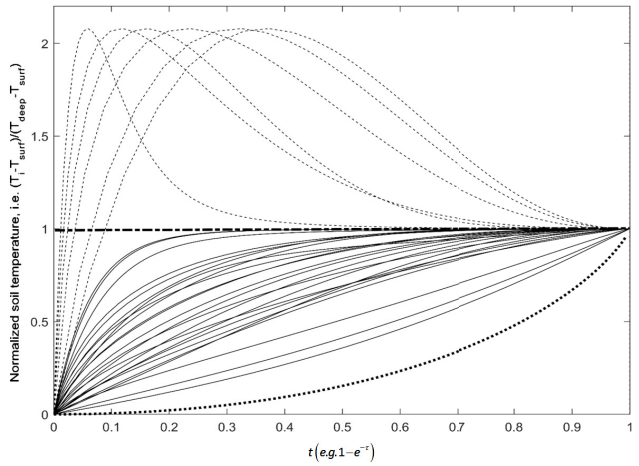

Fig. 2. Soil temperature/moisture profiles combination in $y_{\text{nst}} - x_{1-e^{-\tau}}$ coordinate (solid lines) except soil temperature Case 3 (the dash lines) and 4. $x_{1-e^{-\tau}}$ is defined in (3) and y_{nst} is normalized soil temperature defined in (4). The dotted line is drawn from (8) for a constant $dT/d\tau$ (i.e., the linear case).

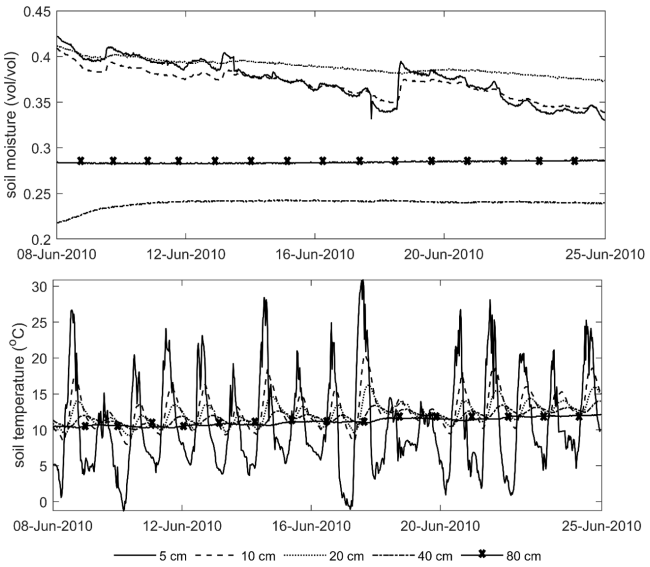

Fig. 3. Time series of inputs. (Top) Soil moisture profile and (Bottom) soil temperature profile.

The equations in the following are developed from the linear case as in [16]. To extend the linear case to the more common nonlinear cases, we approximate the soil temperature profile by adding an exponential decay term to the linear assumption, i.e., $a \to ae^{-\tau}$. Thus, we start with a linear T profile near the surface, which decay gradually to a constant T profile with depth

$$T(\tau) = \int_0^{\tau} (T_{\text{surf}} + ae^{-\tau}\tau)d\tau. \tag{5}$$

So (4) turns to be

$$\begin{aligned}\Delta T_{\text{nor}}(\tau) &= \frac{T(\tau) - T_{\text{surf}}}{T_{\text{deep}} - T_{\text{surf}}} \\ &= \frac{\int_0^{\tau_x} (T_{\text{surf}} + ae^{-\tau}\tau - T_{\text{surf}})d\tau}{\int_0^{\tau_{\text{deep}}} (T_{\text{surf}} + ae^{-\tau}\tau - T_{\text{surf}})d\tau} \\ &= \frac{\int_0^{\tau_x} e^{-\tau}\tau d\tau}{\int_0^{\tau_{\text{deep}}} e^{-\tau}\tau d\tau} \quad (\tau < \tau_{\text{deep}}).\end{aligned} \tag{6}$$

Equation (6) is a dummy format of the linear assumption in (6). Because $\int_0^{\tau_{\text{deep}}} e^{-\tau}\tau d\tau = 1$, then we create a formulas

$$T_{\text{nor}}(\tau) = 1 - e^{-\tau_x} \cdot (\tau_x + 1). \tag{7}$$

Then if we use $t = 1 - e^{-\tau_x}$ to replace τ_x and let $1 - e^{-\tau_{\text{deep}}} \approx 1$, (7) turns into

$$T_{\text{nor}}(t) = 1 - (1-t) \cdot (-\log(1-t) + 1). \tag{8}$$

Equation (8) is actually plotted as the dotted line in Fig. 2.

D. T_{eff} Features in a $y_{nst} - x_{1-e^{-\tau}}$ Coordinate: The Nonlinear Case

Equation (7) is a linear case and all other 24 nonlinear cases could be expressed with adding just one parameter as

$$T_{\text{nor}}(t) = 1 - (1-t)^b \cdot (-\log(1-t) + 1). \tag{9}$$

The values of b corresponds to ΔT_{nor} almost one by one because there are rare crossing points in Fig. 2 among these curves

$$b = \log_{e^{-\tau}} \frac{1 - \Delta T_{\text{nor}}(\tau)}{\tau + 1} = -\frac{1}{\tau} \ln \frac{1 - \Delta T_{\text{nor}}(\tau)}{\tau + 1}. \tag{10}$$

The curve fitting is not shown and hereafter we will prove its efficiency from its inference (Fig. 2). Now, it is possible to infer T_{eff} and the depth (τ) with $T(\tau) = T_{\text{eff}}$ once we know a pair of $(t, \Delta T_{\text{nor}})$ or $(\tau, \Delta T_{\text{nor}})$ because

$$\begin{aligned}T_{\text{eff}} &= \int_0^{\tau_x} T(\tau)e^{-\tau}d\tau \\ &= \int_0^{\tau_x} [(T_{\text{deep}} - T_{\text{surf}}) \cdot \Delta T_{\text{nor}} + T_{\text{surf}}]e^{-\tau}d\tau \\ &= (T_{\text{deep}} - T_{\text{surf}}) \cdot \int_0^1 \Delta T_{\text{nor}}dt + T_{\text{surf}}.\end{aligned} \tag{11}$$

To acquire the soil optical depth where the soil temperature equals T_{eff}(hereafter as $\tau_{T\text{eff}}$), we solve

$$\tau_{T\text{eff}} = -\ln\left(1 - t|_{\frac{T_{\text{eff}}}{T_{\text{deep}} - T_{\text{surf}}} = 1-(1-t)^b \cdot (-\log(1-t)+1)}\right). \tag{12}$$

If T_{eff}, T_{surf}, and T_{deep} are given and the parameter b determined by fitting given profile observations of $T(\tau)$ to the parameterization equation (9), we can infer $\tau_{T\text{eff}}$ via (12). Soil moisture/temperature profiles could be taken from field measurement or from model simulation, while the surface temperature could be retrieved from infrared sensors on satellites or other platform. T_{deep} can be assumed from climatology. Equation (9) postulates a monotonic soil temperature profile with soil optical depth (τ). Once $\tau_{T\text{eff}}$ is estimated, the soil temperature sensing depth can be retrieved from $\tau_{T\text{eff}} = \int_0^{x_{\text{sensing}}} (2\pi/\lambda)(\varepsilon''/\sqrt{\varepsilon'})dx$.

E. In-Situ Data

The Maqu Network locates in Gansu, China, in the northeast margin of the Tibet plateau, and has an average elevation

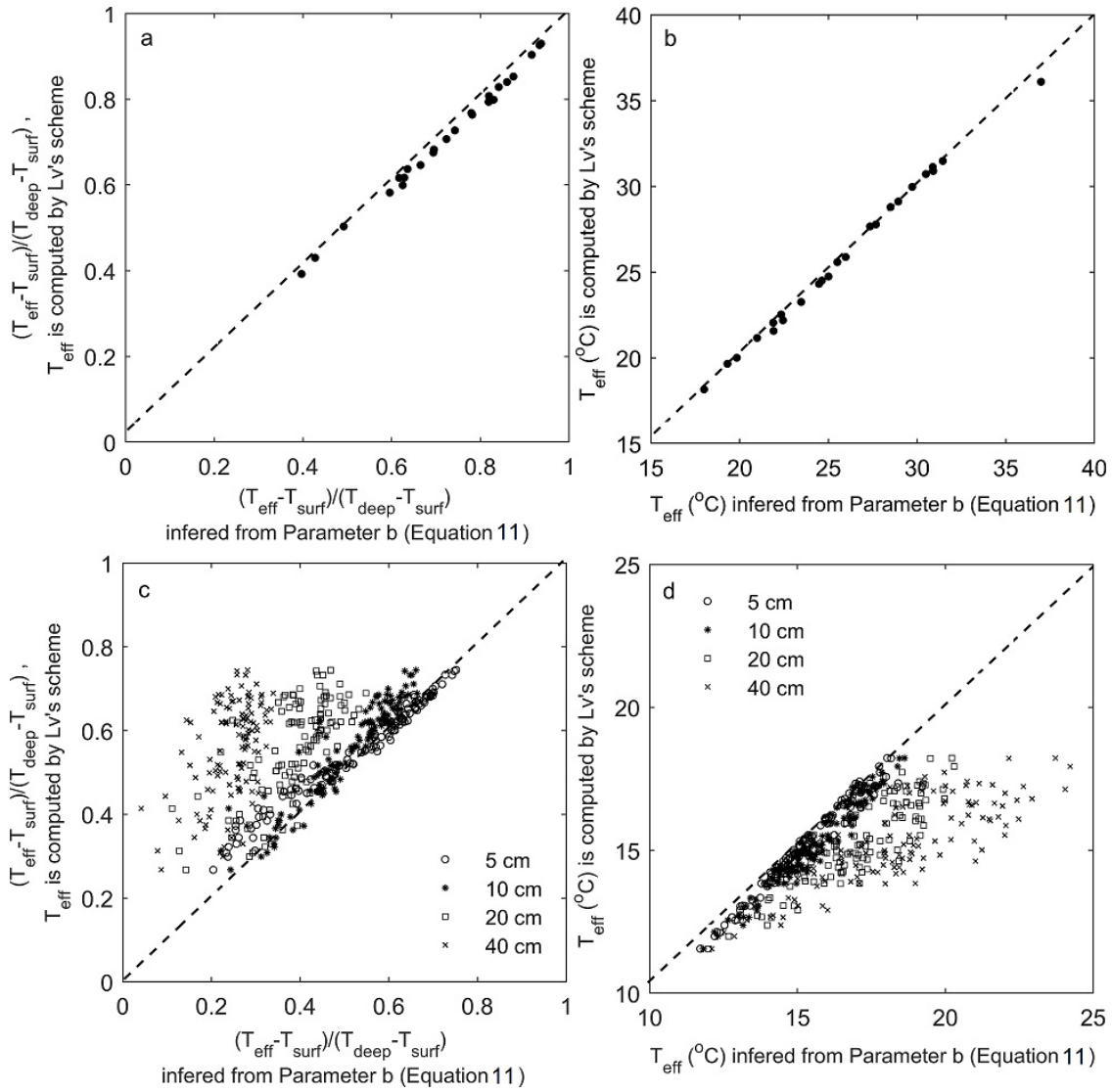

Fig. 4. Normalized Soil effective temperature values inferred from (11) versus the one computed from Lv's scheme for (a) ideal cases in Fig. 1 and (c) field observation at Maqu network from June 8, 2010 to June 25, 2010. Soil effective temperature values inferred from (11) versus the one computed from Lv's scheme for (b) ideal cases in Fig. 1 and (d) field observation at Maqu network from June 8, 2010 to June 25, 2010. Parameter b is calculated from (10) while T_{surf} and T_{deep} are sampled from ideal cases or field observation.

around 3300 m [17], [23]. Vegetation consists of alpine scrublands and meadows, with grass heights less than 1 m and roots extending tens of centimeters in depth. The upper 10 cm of the soil consists of an accumulated humus layer. Shrubs and trees are scarce, while desert dunes sometimes appear along the Yellow River, which runs from the eastern border to its northern border. The Maqu network was installed in 2008. Since then, at least 20 sites of soil moisture/temperature profile observations are being maintained which sufficiently cover one satellite footprint. At each site, soil moisture and temperature probes manufactured by the Decagon Devices Company were deployed. The soil moisture data collected were calibrated according to soil texture and organic content [17], [23]–[25]. Usually, the depth sampling is 5/10/20/40/80 cm, but for some sites, it is only 5/10 cm.

The center station (Fig. 3) measures at 5 cm/10 cm/20 cm/40 cm/80 cm and an infrared sensor provides the surface temperature, so the soil temperature gradient in the top 5 cm can also be inferred. Soil samples are collected near the micrometeorological observing system, which indicates that the soil at 5 cm depth consists of a sand fraction of 26.95% and clay of 9.86%. The fractions are 29.2% and 10.15% at 0.2 m and 31.6% and 10.43% at 0.4 m [26]. In Fig. 3, soil moisture and temperature at 80 cm have almost no diurnal variation. Soil temperature at 5 cm/10 cm/20 cm/40 cm indicates diurnal variation and a phase lag in deeper layers. Soil moisture at 5 cm/10 cm/20 cm is more sensitive to precipitation events and evaporation.

III. Results and Discussion

A. Estimation of T_{eff}

We assume that (9) sufficiently and accurately describes the soil optical depth–soil temperature relationship. Different soil temperature/moisture profile combinations will result in a different parameter b and accurately enough reproduce the true profiles [Fig. 4 (top)]. If we know one point of such a curve,

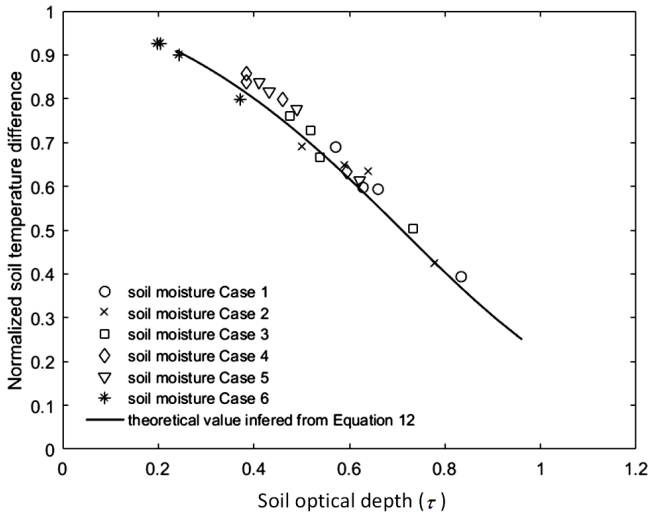

Fig. 5. $\tau_{T\text{eff}}$ estimation from (12) for soil temperature/moisture profiles in Fig. 1 except soil temperature Cases 3 and 4.

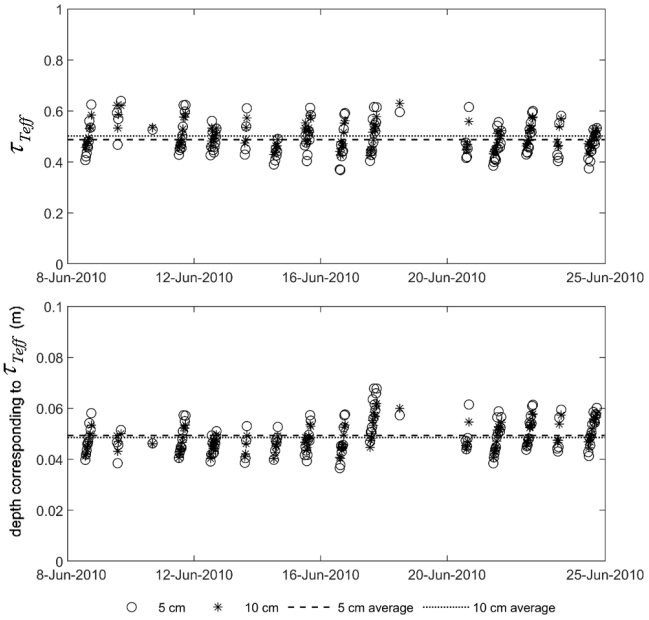

Fig. 6. Time series of (Top) $\tau_{T\text{eff}}$ and (Bottom) its corresponding soil temperature sensing depth. The points are estimation from (12). The depth is computed by $\Delta x = \tau_{T\text{eff}}/((2\pi/\lambda)(\varepsilon''/\sqrt{\varepsilon'}))$.

we know all points. Fig. 4 (bottom) shows the comparison of $(T_{\text{eff}} - T_{\text{surf}}/T_{\text{deep}} - T_{\text{surf}})$ based on the observation shown in Fig. 3. From the theoretical profiles, we may conclude that T_{eff} can be estimated with an error of less than 5% (e.g., 2.5 K if $T_{\text{deep}} - T_{\text{surf}} = 50$ K). Fig. 4 (bottom) shows that for real profiles (as in Maqu), only observation at 5 or 10 cm is usable for this method. Obviously, the strong gradients in soil temperature and soil moisture happen already at that depth range. At deeper layers, soil temperature is already too close to T_{deep}, which presents a sufficiently accurate determination of the parameter b.

B. Estimation of $\tau_{T\,eff}$

For soil temperature Case 3, the gradient is quite small; thus, $T_{\text{eff}} \approx T_i$. The same situation happens for Case 4 which exhibits no soil temperature gradient at all. Fig. 5 shows for all other profiles the soil optical depth $\tau_{T\text{eff}}$ where the soil temperature equals T_{eff}. The points follow the theoretical estimation line [see (12)]. It should be noted that τ in this paper is computed by Peplinski's dielectric mixing model [27].

While Fig. 5 shows the ideal cases in Fig. 1, the result in Fig. 6 show the application of (12) to the field measurement. Fig. 6 shows the time series for cases with monotonic soil temperature profiles. This condition is usually satisfied from 10 A.M. to 6 P.M. because after sunrise, the soil temperature gradient increases. For liner T profiles, $\tau_{T\text{eff}}$ is the penetration depth. Our results show, however, that the average $\tau_{T\text{eff}}$ is around 0.5, and values may vary between 0.4 and 0.5. The corresponding average geometric depth is 5 cm and varies from 4 to 6 cm, i.e., soil temperature sensing depth is where its soil temperature equals T_{eff}. The overpassing times of SMOS [2] and SMAP [1] are around at 6 A.M. and 6 P.M.; however, the average $\tau_{T\text{eff}}$ (and its geometric depth) does not coincide with $\tau_{T\text{eff}}$ during the overpassing times of the satellites. To investigate $\tau_{T\text{eff}}$ and its corresponding depth during the satellite overpassing time, it requires that the monotonic condition is satisfied. It is nevertheless possible to find a depth where the soil temperature equals to T_{eff} by the method introduced in this paper, and as such, it may give some clues to find where the soil moisture equals to what is retrieved from the satellites.

C. Application to SMAP

Surface soil temperature is available from satellite observation, and deep soil temperature can be inferred from the average of soil temperature at deeper layers from models. As T_{eff} is the equivalent soil temperature and the soil moisture retrieved from zeroth-order incoherent model represents the effective emissivity in (1), one may use T_{eff} and the satellite soil moisture product to estimate the soil temperature sensing depth.

Fig. 7 shows the estimated soil temperature sensing depth map at L-band with the soil effective temperature calculated by MERRA-2 and the SMAP L3 soil moisture for the overpassing times at 6 A.M. and 6 P.M. For most of the area, the soil temperature sensing depth is around 0.05–0.1 m [Fig. 7(a), (b), (g), and (h)]. Extreme cases appear in the subtropical zones such as North Africa, Australia, Central Asia, and Southern Africa. Among these regions, only the North Africa and the Central Asia persistently result in soil temperature sensing depths of more than 20 cm because of the dry conditions [Fig. 7(c) and (d)]. For the rest area, the soil temperature sensing depth is reduced to about 5 cm once it rains. Fig. 7(e) and (f) shows that the soil temperature sensing depth usually does not reach deeper than 0.1 m except for the subtropical zones and other dry areas. Lv *et al.* [16] showed that the major contributing layers can reach 0.3–0.4 m in terms of T_{eff} computation, so it is reasonable for subtropical zones and other dry areas the soil temperature sensing depth can be that deep. The minimum/maximum values are controlled by

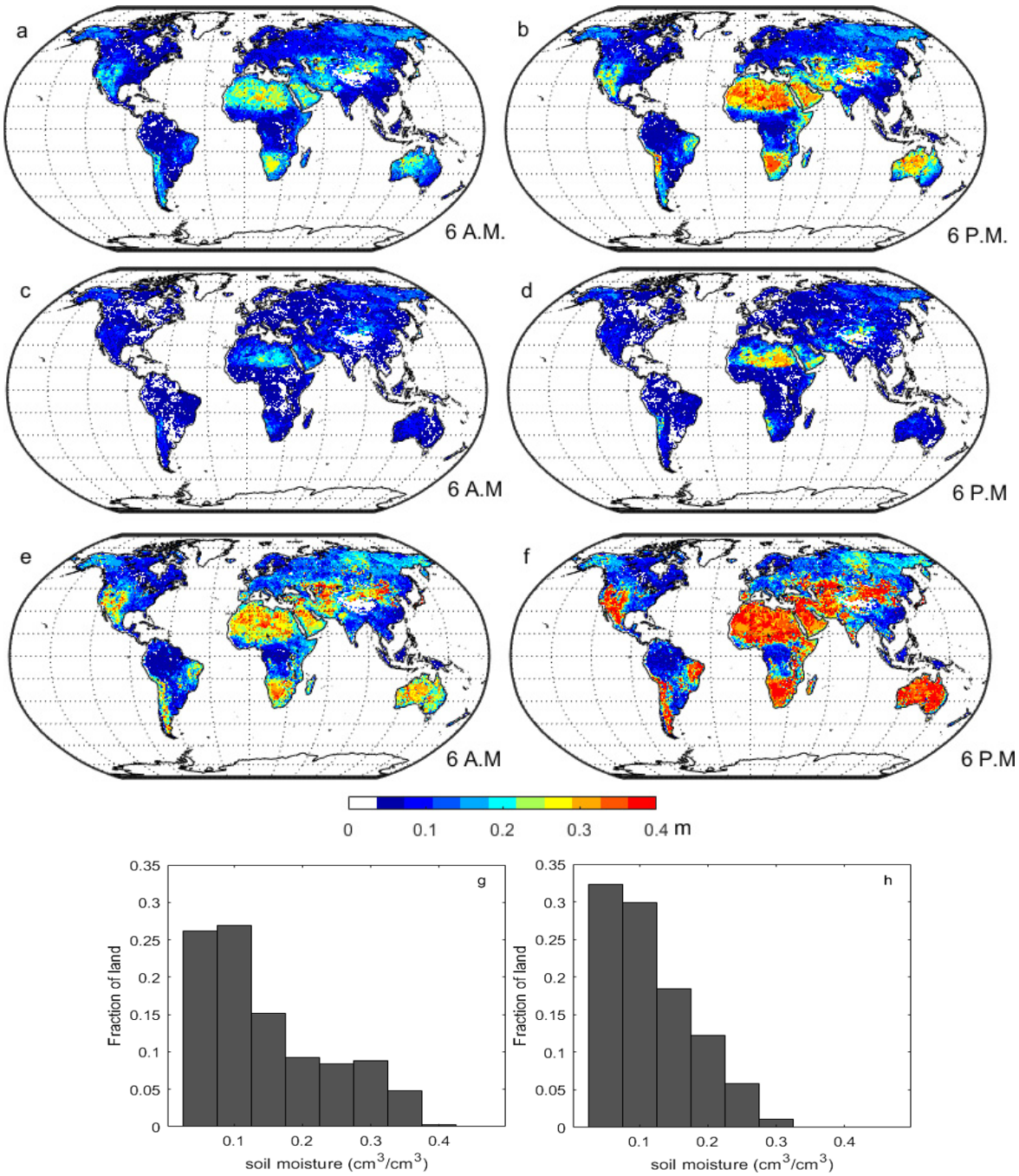

Fig. 7. Global map of soil temperature sensing depth. (a) Mean at 6 A.M. local time. (b) Mean at 6 P.M. local time. (c) Minimum at 6 A.M. local time minimum. (d) Minimum at 6 P.M. local time. (e) Maximum at 6 A.M. local time. (f) Maximum at 6 P.M. local time. (g) and (h) Histograms of the maps in (a) and (b).

the variation of soil moisture. The variation of soil temperature sensing depth should be taken into account where the annual soil moisture variation is strong (Fig. 8). When surface soil is wet, T_{eff} is close to the surface temperature value. On the opposite, T_{eff} approaches the deep soil temperature if the surface soil is dry. It should be noted that soil temperature sensing depth was also computed on equatorial forests, while on such targets accounting for a contribution of soil to the total emission is quite challenging at L-band. Here, we estimate the soil temperature sensing depth at equatorial forests as long as SMAP does not blank out these regions and offers the soil moisture retrievals.

In this paper, we distinguish soil temperature sensing depth and penetration depth while Ulaby *et al.* [9] assumed that both are identical. Lv *et al.* [16] described in detail how the map of penetration depth was obtained. Fig. 9 gives a global map of the difference between both, which shows that the penetration depth is always deeper than the soil temperature sensing depth. The difference can reach 10 cm at 6 A.M. but only 2 cm at 6 P.M. because the soil temperature profile is monotonic

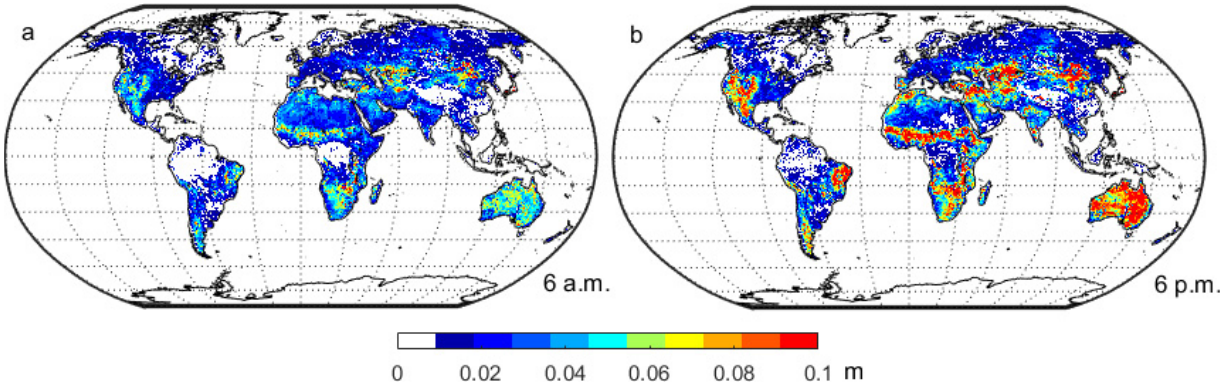

Fig. 8. Global map of soil temperature sensing depth standard deviation (RMSD) for (a) 6 A.M. and (b) 6 P.M.

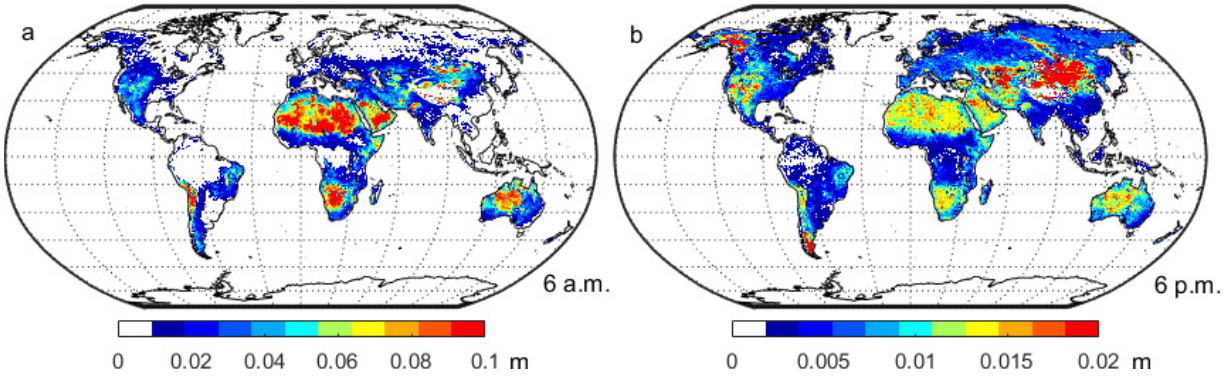

Fig. 9. Mean difference between penetration depth and soil temperature sensing depth (penetration depth minus soil temperature sensing depth) for (a) 6 A.M. and (b) 6 P.M. White areas over land mean the soil temperature never fits the monotonic assumption through the year.

in the latter case. Main differences appear in the subtropics. It should be noted that the same method could also be applied to SMOS, Aquarius, or future L-band satellites, together with their corresponding ancillary data. On the other hand, since MERRA-2 contains seven layers of soil temperature and (9) has a strict requirement for the input soil temperature profile, we only show here the application of our method to SMAP data.

IV. Conclusion

This paper aims to improve our understanding of the assumptions and hypothesis when simplifying the incoherent model to a coherent model. In particular, we developed an objective method to estimate the soil temperature sensing depth, i.e., the depth at which the soil temperature equals the soil effective temperature in the incoherent model. The soil temperature and soil moisture profiles in Fig. 1 are referenced from Ulaby *et al.* [9] and Njoku and Kong [22]. These are typical cases that stand for all kinds of profile states. The method developed in Section II does not depend on any local parameters, because both ΔT_{nor} and soil optical depth τ are not site-dependent. It is the dielectric constant models that require clay/sand fraction or others as inputs. These parameters should keep consistent with the one used in SMAP/SMOS retrieval techniques as in Section III-C. In the incoherent model, just one layer is assumed to represent the soil moisture retrieved from L-band satellites (i.e., one brightness temperature value corresponds to one emissivity, therefore, one soil moisture value). Such assumption challenges our understanding about the depth the satellite is actually observing. The effective soil temperature depends on the profiles of soil temperature and soil moisture; thus, the information on which layer the satellites are sensing is possibly hidden in the T_{eff} scheme. Here, we revisited the concepts of penetration depth and soil temperature sensing depth, which is only identical when T varies linearly with soil optical depth. For nonlinear but still monotonous cases, the method developed here can be useful.

The new T_{eff} model proposed by Lv *et al.* [14] is a flexible approximation to Wilheit's model, which easily accommodates arbitrary layering assumptions, which can reach from two layers as the minimum to as many layers as needed while approaching the accuracy of Wilheit's model. Thus, the scheme can be easily applied to field observation and model output. In this paper, a semiempirical model is developed to describe the common features of various soil moisture/temperature profile combinations. With this model, it is possible to identify the relationship between geometric soil depth, penetration depth, and the soil temperature sensing depth and allows further understanding on which depth SMOS and SMAP are really observing.

As a final note, we would like to highlight that the problem about where the satellites are observing still needs extensive research. To investigate this problem further, the detailed soil moisture and soil temperature profiles are needed as well as

corresponding ground-based radiometer observations, to be deployed across different climate zones. Only in this way, we can exclude other influence factors such as scale, subpixel landscape mixture, and RFI. Furthermore, the observation period should cover years and seasons, and must not be limited by the satellites' overpassing times.

REFERENCES

[1] A. Colliander *et al.*, "Validation of SMAP surface soil moisture products with core validation sites," *Remote Sens. Environ.*, vol. 191, pp. 215–231, Mar. 2017.

[2] J. P. Wigneron *et al.*, "Modelling the passive microwave signature from land surfaces: A review of recent results and application to the L-band SMOS & SMAP soil moisture retrieval algorithms," *Remote Sens. Environ.*, vol. 192, pp. 238–262, Apr. 2017.

[3] Y. H. Kerr *et al.*, "The SMOS soil moisture retrieval algorithm," *IEEE Trans. Geosci. Remote Sens.*, vol. 50, no. 5, pp. 1384–1403, May 2012.

[4] D. Entekhabi *et al.*, "The Soil Moisture Active Passive (SMAP) mission," *Proc. IEEE*, vol. 98, no. 5, pp. 704–716, May 2010.

[5] B. Peng *et al.*, "Reappraisal of the roughness effect parameterization schemes for L-band radiometry over bare soil," *Remote Sens. Environ.*, vol. 199, pp. 63–77, Sep. 2017.

[6] P. J. Shellito *et al.*, "SMAP soil moisture drying more rapid than observed *in situ* following rainfall events," *Geophys. Res. Lett.*, vol. 43, pp. 8068–8075, Aug. 2016.

[7] M. J. Escorihuela, A. Chanzy, J. P. Wigneron, and Y. H. Kerr, "Effective soil moisture sampling depth of L-band radiometry: A case study," *Remote Sens. Environ.*, vol. 114, pp. 995–1001, May 2010.

[8] F. C. Zhou, X. Song, P. Leng, and Z. L. Li, "An effective emission depth model for passive microwave remote sensing," *IEEE J. Sel. Topics Appl. Earth Observ. Remote Sens.*, vol. 9, no. 4, pp. 1752–1760, Apr. 2016.

[9] F. T. Ulaby, R. K. Moore, and A. K. Fung, *Microwave Remote Sensing Active and Passive: From Theory to Applications*, vol. 3. Norwood, MA, USA: Artech House, 1986.

[10] T. T. Wilheit, "Radiative transfer in a plane stratified dielectric," *IEEE Trans. Geosci. Remote Sens.*, vol. GRS-16, no. 2, pp. 138–143, Apr. 1978.

[11] B. J. Choudhury, T. J. Schmugge, and T. Mo, "A parameterization of effective soil temperature for microwave emission," *J. Geophys. Res., Oceans Atmos.*, vol. 87, pp. 1301–1304, Feb. 1982.

[12] J. P. Wigneron, L. Laguerre, and Y. H. Kerr, "A simple parameterization of the L-band microwave emission from rough agricultural soils," *IEEE Trans. Geosci. Remote Sens.*, vol. 39, no. 8, pp. 1697–1707, Aug. 2001.

[13] T. R. H. Holmes *et al.*, "A new parameterization of the effective temperature for L band radiometry," *Geophys. Res. Lett.*, vol. 33, p. L07405, Apr. 2006.

[14] S. Lv, J. Wen, Y. Zeng, H. Tian, and Z. Su, "An improved two-layer algorithm for estimating effective soil temperature in microwave radiometry using *in situ* temperature and soil moisture measurements," *Remote Sens. Environ.*, vol. 152, pp. 356–363, Sep. 2014.

[15] S. Lv, Y. Zeng, J. Wen, and Z. Su, "A reappraisal of global soil effective temperature schemes," *Remote Sens. Environ.*, vol. 183, pp. 144–153, Sep. 2016.

[16] S. Lv, Y. Zeng, J. Wen, H. Zhao, and Z. Su, "Estimation of penetration depth from soil effective temperature in microwave radiometry," *Remote Sens.*, vol. 10, no. 4, p. 519, 2018.

[17] Z. Su *et al.*, "The Tibetan Plateau observatory of plateau scale soil moisture and soil temperature (Tibet-Obs) for quantifying uncertainties in coarse resolution satellite and model products," *Hydrol. Earth Syst. Sci.*, vol. 15, no. 7, pp. 2303–2316, 2011.

[18] Y. J. Zeng, L. Wan, Z. Su, H. Saito, K. Huang, and X. Wang, "Diurnal soil water dynamics in the shallow vadose zone (field site of China University of Geosciences, China)," *Environ. Geol.*, vol. 58, pp. 11–23, Jul. 2009.

[19] Y. Zeng *et al.*, "Diurnal pattern of the drying front in desert and its application for determining the effective infiltration," *Hydrol. Earth Syst. Sci.*, vol. 13, pp. 703–714, Jun. 2009.

[20] Y. Zeng, Z. Su, L. Wan, and J. Wen, "Numerical analysis of air-water-heat flow in unsaturated soil: Is it necessary to consider airflow in land surface models?" *J. Geophys. Res., Atmos.*, vol. 116, p. D20107, Oct. 2011.

[21] Y. J. Zeng, Z. B. Su, L. Wan, and J. Wen, "A simulation analysis of the advective effect on evaporation using a two-phase heat and mass flow model," *Water Resour. Res.*, vol. 47, p. W10529, Oct. 2011.

[22] E. G. Njoku and J.-A. Kong, "Theory for passive microwave remote sensing of near-surface soil moisture," *J. Geophys. Res.*, vol. 82, pp. 3108–3118, Jul. 1977.

[23] Z. Su, P. de Rosnay, J. Wen, L. Wang, and Y. Zeng, "Evaluation of ECMWF's soil moisture analyses using observations on the Tibetan Plateau," *J. Geophys. Res., Atmos.*, vol. 118, no. 11, pp. 5304–5318, 2013.

[24] L. Dente, Z. Vekerdy, J. Wen, and Z. Su, "Maqu network for validation of satellite-derived soil moisture products," *Int. J. Appl. Earth Observ. Geoinf.*, vol. 17, pp. 55–65, Jul. 2012.

[25] L. Dente, Z. Su, and J. Wen, "Validation of SMOS soil moisture products over the Maqu and Twente regions," *Sensors*, vol. 12, no. 8, pp. 9965–9986, 2012.

[26] H. Zhao, Y. Zeng, S. Lv, and Z. Su, "Analysis of soil hydraulic and thermal properties for land surface modeling over the Tibetan Plateau," *Earth Syst. Sci. Data*, vol. 10, no. 2, p. 1031, 2018.

[27] N. R. Peplinski, F. T. Ulaby, and M. C. Dobson, "Dielectric properties of soils in the 0.3-1.3-GHz range," *IEEE Trans. Geosci. Remote Sens.*, vol. 33, no. 3, pp. 803–807, May 1995.

Shaoning Lv received the Ph.D. degree from the Northwest Institute of Eco-Environment and Resources, Chinese Academy of Sciences, Lanzhou, China, in 2014. He is currently pursuing the Ph.D. degree with the Water Resources Department, Faculty of Geo-Information Science and Earth Observation, University of Twente, Enschede, The Netherlands.

His research interests include passive microwave remote sensing of soil moisture and its application in climate forecast.

Yijian Zeng received the Ph.D. degree from the University of Twente, Enschede, The Netherlands, in 2012.

He is currently an Assistant Professor with the Water Resources Department, Faculty of Geo-Information Science and Earth Observation, University of Twente. His research interests include land–atmosphere interaction via hydrologic processes and how the interaction affects the climate system, generation of consistent climate data record using multisources of geo-datasets, physical mechanisms of land surface models, and the application of data assimilation.

Zhongbo (Bob) Su received the M.Sc. degree in hydrological engineering from IHE, Delft, The Netherlands, in 1989, and the Ph.D. degree in civil engineering from Ruhr University, Bochum, Germany, in 1996.

He is currently a Professor of spatial hydrology and water resources management and the Chairman of the Department of Water Resources, Faculty of Geo-Information Science and Earth Observation, University of Twente, Enschede, The Netherlands. His research interests include remote sensing and numerical modeling of land surface processes and interactions with the atmosphere, earth observation of water cycle and applications in climate, ecosystem and water resources studies, and monitoring food security and water-related disasters.

Jun Wen received the B.A. degree in meteorology from Peking University, Beijing, China, in 1988, the M.A. degree in meteorology from Lanzhou University, Lanzhou, China, in 1995, and the Ph.D. degree in meteorology from the Chinese Academy of Sciences, Lanzhou, in 1999.

He is currently a Professor with the College of Atmospheric Sciences, Chengdu University of Information Technology, Chengdu, China. His research interests include remote sensing and data assimilation, land surface modeling, and climate change.